Lei Sang, Shuaitao Li, Bin Hu, Kehan Dai, Mark Kraman, Hong Yang, and Wen Huang

Reconfigurable Microstrip Patch Antennas on Flexible Substrates

A design method.

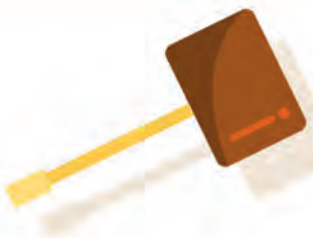

This article elaborates on the general design route of stretchable microstrip patch antennas, which are fabricated on polydimethylsiloxane (PDMS) soft substrates. Compared to conventional counterparts on rigid substrates, the stretchability brings about the change of both the overall physical dimensions and the electrical parameters of the materials. Being different from the traditional design route, the deformation parameters are involved into the classical design equations of the microstrip patch antenna. Based on the improved equations, the reconfigurable antenna is able to work at multiple frequency points by using a comprehensive optimization algorithm. For demonstrative purpose, a microstrip patch antenna on PDMS is designed, fabricated, and measured. The demonstrative patch antenna shows nearly the same electrical performance as expected from finite-element method modeling when the center operating frequency is tuned from 6 to 4.9 GHz under a strain of up to 20%. Compared with the simulated results of a conventional design with strain of 5% to 20%, the realized gains have increased by 0.9 dBi (0% strain at 6 GHz), 0.9 dBi (5% strain at 5.7 GHz), 1.9 dBi (15% strain at 5.2 GHz), and 0.8 dBi (20% strain at 4.9 GHz), respectively, by using the strain domain involved design method.

Digital Object Identifier 10.1109/MAP.2023.3301387
Date of current version: 24 August 2023

INTRODUCTION

With the rapid development of a diverse variety of electronic technologies, such as bionic robots [1] [2], wearable electronics [3], [4], and artificial organs [5], [6], there is an ever-increasing demand to fabricate electronic systems that are mechanically flexible [7], [8]. However, as a central component in wireless communication systems, high-frequency circuits fabricated on rigid substrates are unable to meet this new standard [9], [10]. Therefore, in the past decade, novel circuits demonstrated on elastomer materials have attracted widespread attention and have been developing rapidly, especially for dc and

1045-9243/23©2023IEEE

low-frequency applications [11], [12]. However, trends in technology development require higher operating frequencies to facilitate wider communication bandwidth, which challenges microwave devices and circuit designs on stretchable substrates under complex forms of deformation [13], [14]. For flexible devices, the elasticity of the substrate has the greatest influence on the design of the microwave antenna. Many important issues remain unsolved, such as how to adjust the traditional antenna design paradigm to accommodate the properties of elastic substrates [15], [16], [17].

For flexible devices, the elasticity of the substrate has the greatest influence on the design of the microwave antenna.

Naturally, a stretchable microstrip patch antenna is reconfigurable. Narrow-band stretchable antennas can be highly sensitive to substrate deformation and need to be discussed more strictly, while relative insensitivity of wide-band antennas to substrate deformation can be assumed. Considering that mainstream wireless communication systems, such as wireless local area network 5.8-GHz frequency band, is divided into multichannels from 5.15 to 5.85 GHz, a slight deformation of the substrate and the conductive layer could have a significant impact on the performance of the antenna and the electronic system [18], [19]. Therefore, according to the requirements of the above application scenario, it is important to develop a design route for stretchable antennas to properly consider the dynamic dimensions and the dynamic parameters of the material's properties accordingly [20], [21]. The performance of the antenna will then become a function of not only the frequency, but also a function of the strain. At present, most of the achievements of stretchable antennas are focused on elastic materials, such as in [18], [19], [20], [21], [22], [25], [26], [27], [28], and [29]. Other studies take the change of tensile length into account, but ignore the change of other deformation dimensions or the change of material electrical parameters when the substrate is stretched [22], [23], [24].

Taking into account all of the variations of physical dimensions and the change of material electrical parameters induced by stretching, in this article a general design method involving the strain domain for stretchable microstrip patch antennas is proposed. The theoretical relationship between the antenna performance and the deformation parameters are established. As a result, the initial sizes of the soft antenna are able to be optimized, especially when there are multireconfigurable operating frequency points. Compared to traditional design methods, there are two novel concepts in this article:

- The deformation parameters are involved into the antenna design equations. In addition, the effective dielectric constant (ε) and equivalent conductivity (σ) are both considered to be dependent variables of the deformation parameters.
- Based on the improved equations, a novel design flow of reconfigurable soft antennas is given in this article.

With the improved design method, the initial sizes of the soft antenna and the stretching scale is able to be optimized by using the improved equations and design flow in the article.

To demonstrate the design route, the design of a reconfigurable microstrip patch antenna is chosen as an example. As for the choice of substrate materials, PDMS has good tensile property of more than 50%, suitable relative dielectric constants of 2 to 5, and good skin affinity, which make it an excellent material for the fabrication of high-frequency stretchable antennas [25], [26], whereas conventional conductor layers have almost no obvious tensile properties [27], [28]. To improve the tensile property of the conductor layer, the "prestrained" processing is used in the fabrication of the conductive layer [29].

DESIGN ROUTE FOR A STRETCHABLE SOFT ANTENNA

$$L = L_0 \times (1 + St) \tag{1}$$

$$W = W_0 - \rho \times St \times W_0 \tag{2}$$

$$H = \frac{L_0 W_0 H_0}{LW}. \tag{3}$$

Compared to the design route of a conventional flexible antenna, there is, in addition to the frequency domain, the strain domain that needs to be considered throughout the design of a stretchable antenna. Besides the effect on the physical dimensions of the antenna itself, the strain domain is critical due to the transformation of the dielectric and conductive material properties from constants to strain-dependent values. As the electrical performance of the antenna is related to the structural dimensions, stretchable antennas are characteristically reconfigurable microwave devices. The general design strategy aims to achieve the best overall electrical performance at all desired operating frequencies. By engineering the strain needed at each frequency to achieve the desired performance relative to the initial physical dimensions of the antenna, optimum overall performance can be achieved. As shown in Figure 1, the design route could be divided into five main steps.

1) Determine the quantitative relationship between the strain ratio and the physical dimensions of the soft patch antenna.
2) Determine the quantitative relationship between the strain ratio and the material electrical parameters, like the conductivity of the conductive layer and relative dielectric constant of the soft substrate.
3) Based on the quantitative relationships derived above, determine the optimum initial structure dimensions of the

radiation patch under normal state to achieve the best average add-up performance at all reconfigurable frequency points under strained states.

4) Based on the initial structure dimensions of the radiation patch, design a feeding line that applies to each reconfigurable frequency point.
5) Build the 3D model and evaluate the performance of the soft patch antenna by using the electromagnetic and mechanical cosimulation. In the cosimulation, frequency and strain ratio are both the scanning parameters.

Compared to the design route of a conventional flexible antenna, there is, in addition to the frequency domain, the strain domain that needs to be considered throughout the design of a stretchable antenna.

Taking a stretchable patch antenna on a PDMS substrate as an example, the detailed step-by-step design route considering the frequency and the strain domains simultaneously is illustrated below. For the first step, the quantitative relationship among outline dimensions (length L, width W, and thickness H) of the PDMS substrate are calculated by (1) to (3), while the strain is applied uniaxially along the direction of the electromagnetic wave transmission. St is the strain ratio parameter, ρ is the Poisson coefficient; L_0, W_0, and H_0 are the length, width, and thickness of the PDMS substrate under the normal state, respectively.

Although the outline of the whole soft substrate is linear with the strain ratio, the deformation is not completely uniform on the whole substrate according to the simulated results with Ansys Workbench [shown in Figure 2(a)]. Corresponding to the position of the stretching PDMS substrate, the straining change curves of the antenna structure parameters are derived, as shown in Figure 3.

The next step is to acquire the change curves of the critical material electrical parameters varied with the strain. As metal layer will crack with the stretching, the conductivity of the metal layer will decline rapidly [30]. The numerical values of the conductivity of the stretched conductor layer were tested by using the probe method, as shown in Figure 4(a). Due to the prestrain process, the downward trend of the conductivity is mitigating. The conductivity is about 10^6 S/m when strain ratio is 20%. Another parameter is the relative dielectric constant of the PDMS. The numerical values of the relative dielectric constant of the PDMS shown in Figure 4(b) were measured using a Keysight dielectric probe kit. The relative dielectric constant is 2.7 under normal state, while it increases to 2.95 when the strain ratio is 35%.

Figure 5 shows the direct observation of the surface morphology of the Au/Ni metal conductor layer under different biaxial poststrain conditions. Under a high-magnification optical microscope, the surface morphology of the Au/Ni metal offers an appearance akin to a "fishing net" at the micrometer scale in Figure 5(a). Under a larger poststrain of 25% as shown in Figure 5(b), the "fishing net" contains smaller crack domains. However, the size of discontinuities between domains changes minimally and is negligibly small compared to the operating wavelength of the antenna in the gigahertz range. Radio frequency (RF) signals are able to pass across the discontinuities between metal domains easily by large electrical field coupling. If we want to repair the cracks and improve the conductivity, we can also brush the stretched surface with an elastic conductive liquid like electrical conductive composites.

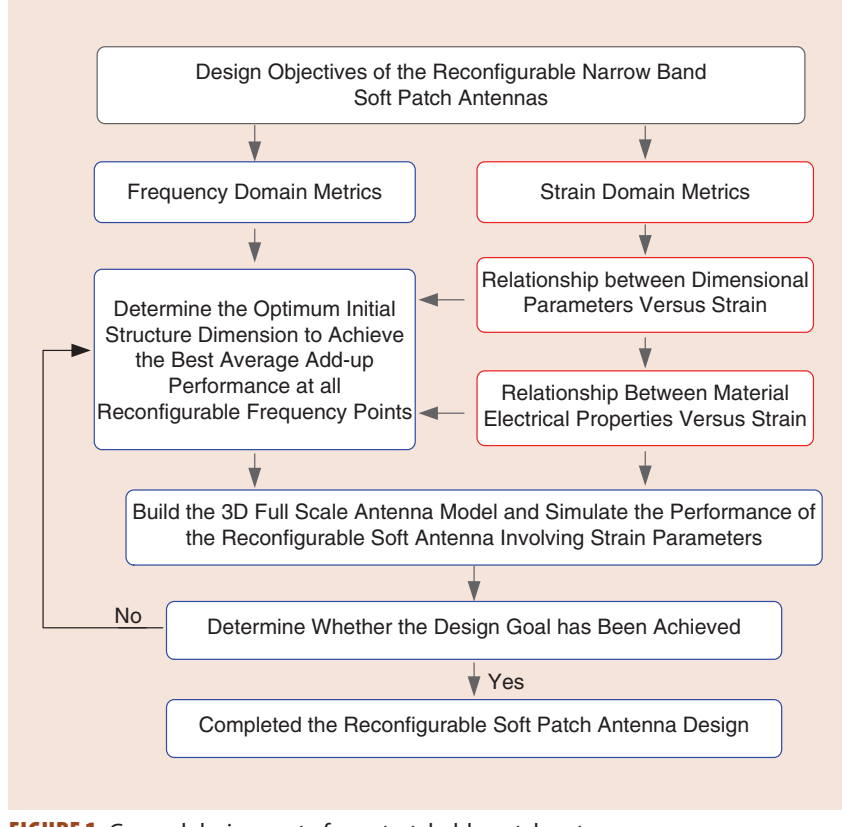

FIGURE 1. General design route for a stretchable patch antenna.

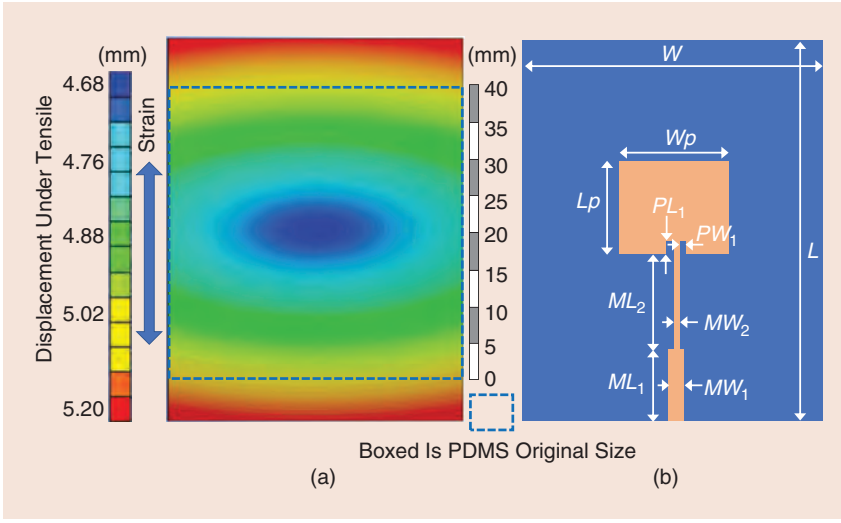

FIGURE 2. Schematic view of the structure of a stretchable patch antenna after the tensile is applied in the indicated direction. (a) Simulated displacement of the PDMS substrate under the tensile in Ansys Workbench. (b) The configuration and critical dimensions of the patch antenna.

The next step is to determine the range and initial dimensions of the stretchable patch antenna with consideration of the desired operating frequency, bandwidth, and maximum allowable strain, which, in this work, are set to be within the popular commercial wireless frequency band from 4.9 to 6 GHz, with a step size of ~0.3 GHz, a bandwidth of 100 MHz, and strain of 35% (permissible maximum strain ratio), respectively. Therefore, the lowest limit of the patch antenna's initial length $L_{p,\min}$ and width $W_{p,\min}$ are determined with the maximum operating wavelength at 4.9 GHz, when the substrate is strained to 35%, i.e., the maximum strain specification. In this case, the initial patch antenna length $L_{p,\min} \times 1.35$ should be larger than half

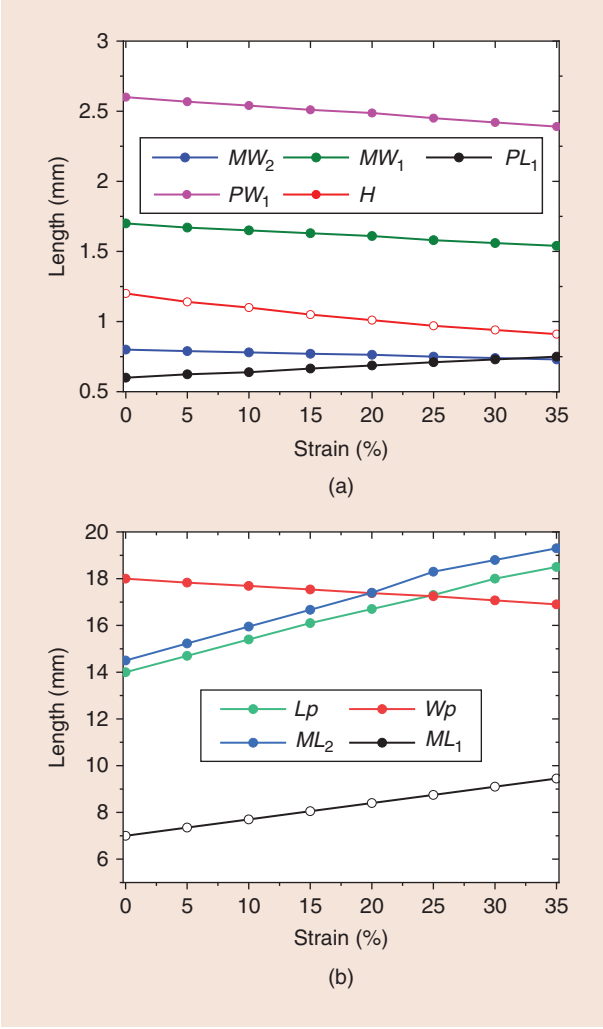

FIGURE 3. Straining change curves of the antenna structure parameters.

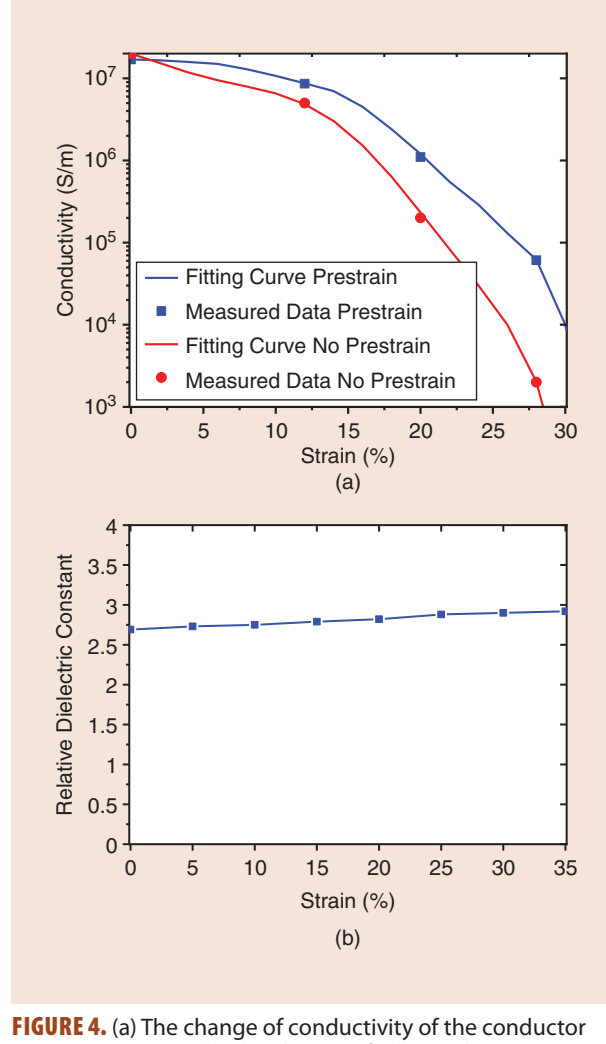

FIGURE 4. (a) The change of conductivity of the conductor layer versus strain. (b) The change of relative dielectric constant versus strain.

of the maximum wavelength at 4.9 GHz. Oppositely, the upper limit of the patch antenna length $L_{p,\max}$ and the width $W_{p,\max}$ can be calculated by the minimum operating wavelength at 6 GHz and a strain of 0%. Involving the strain ratio parameters S to the conventional design equations for patch antennas and the above limitations, the values of $L_{p,\min}$, $W_{p,\min}$, $L_{p,\max}$, and $W_{p,\max}$ can be calculated using (4) to (10), shown below.

$$L_{p,\min} = \frac{1}{2f_{\max} \times (1+St)\sqrt{\varepsilon_{\text{eff}}\mu_0\varepsilon_0}} - 2\Delta L \tag{4}$$

$$W_{p,\min} = \frac{1}{2f_{\max}(1-\rho \times St)\sqrt{\mu_0\varepsilon_0}}\sqrt{\frac{2}{\varepsilon_r(St)+1}} \tag{5}$$

$$L_{p,\max} = \frac{1}{2f_{\min} \times \sqrt{\varepsilon_{\text{eff}}\mu_0\varepsilon_0}} - 2\Delta L \tag{6}$$

$$W_{p,\max} = \frac{1}{2f_{\min}\sqrt{\mu_0\varepsilon_0}}\sqrt{\frac{2}{\varepsilon_r(St)+1}} \tag{7}$$

$$\varepsilon_{\text{eff}} = \frac{\varepsilon_r(St)+1}{2} + \frac{\varepsilon_r(St)-1}{2}\left[1+12\frac{H(St)}{W_p}\right]^{-\frac{1}{2}} \tag{8}$$

$$\Delta L = 0.412 \times H(St)\frac{(\varepsilon_{\text{reff}}+0.3)\left(\frac{W_p}{H(St)}+0.264\right)}{(\varepsilon_{\text{reff}}-0.258)\left(\frac{W_p}{H(St)}+0.8\right)} \tag{9}$$

$$R_c = \sqrt{\frac{\omega\mu_0}{2\sigma(St)}} \tag{10}$$

in which, the conductivity $\sigma(St)$ and relative dielectric constant $\varepsilon r(St)$ change with the strain of the substrate, as shown in Figure 4. Rc is the resistance loss introduced by a metal patch. ΔL is a correction factor for the edge truncation effect of the electromagnetic field. The calculated values of $L_{p,\min}$, $W_{p,\min}$, $L_{p,\max}$, and $W_{p,\max}$ are 12, 16, 16, and 20 mm, respectively. The differences with the traditional equations are as follows:

- The deformation parameters St and the Poisson's coefficient of the soft substrate are involved into the traditional patch antenna equations.
- The effective dielectric constant and equivalent conductivity are both functions of the deformation parameters.
- The antenna performance is not only dependent on the frequency but also sensitive to the deformation parameters St.

With a step size of 0.5 mm for patch antenna length L_p and width W_p in the above corresponding range, the desired electrical performance is then evaluated on all possible combinations of values of L_{p0} and W_{p0} by only modeling the patch structure with two assumptions:

- perfect matching to a 50 Ω input port
- no parasitic effects are introduced by the feedline, in high-frequency structure simulator (HFSS).

Among typical antenna performances, such as the antenna gain, return loss, radiation pattern, efficiency, etc., the desired performance could be different depending on the application scenario. Therefore, an evaluation parameter $Z_{Lpn,Wpn}$ is defined to represent the overall performance of a stretchable patch antenna with the nth initial physical dimension combination of L_{p0} and W_{p0}.

$$Z_{LpnWpn} = q_1 \times \text{Return loss} + \text{Gain} + q_3 \times \text{Efficiency} + \ldots, \tag{11}$$

where $q_1, q_2, q_3, \ldots$ are weight coefficients. In this work, other than $q_1 = 1$, all of the other weight coefficients are zero to simplify the demonstration. At each desired operating frequency point, the value of the evaluation parameter $Z_{Lpn,Wpn}$ is calculated as shown in Figure 6.

Then, an optimum combination of stretchable patch antenna with initial length L_{p0} of 14 mm and width W_{p0} of 18 mm is found where the $\Sigma_{f1}^{f5} Z_{Lpn,Wpn}(f)$ the maximum value of 19.81 dB, and f represents the desired discrete operating frequency points array of {f_1 = 4.9 GHz, f_2 = 5.2 GHz, f_3 = 5.4 GHz, f_4 = 5.7 GHz, f_5 = 6.0 GHz}. The corresponding discrete strain points array is {St_1 = 20% at f_1, St_2 = 15% at f_2, St_3 = 10% at f_3, St_4 = 5% at f_4, St_5 = 0% at f_5}.

The next critical design step is to determine the type of antenna feedline and its initial physical dimension. Knowing the optimum dimensions of the patch, the input impedance [$Z_p(f)$] at the junction of the patch and feedline shown in Figure 2 can be calculated by (12) to (14):

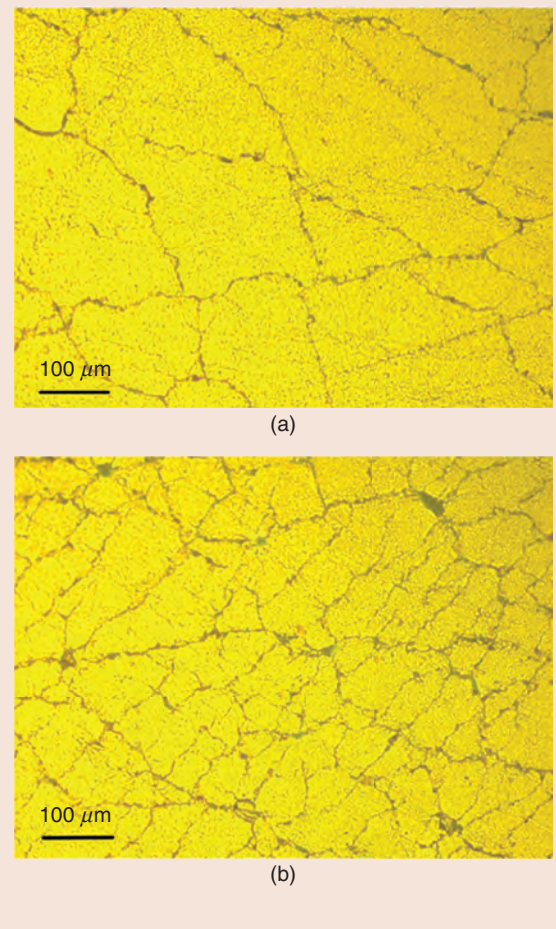

FIGURE 5. The size comparison of cracked microdomains under different strain magnitudes. (a) Biaxial strain of 10%; (b) biaxial strain of 25%.

$$Z_p = \frac{1}{2(G_1 + G_2)} \tag{12}$$

$$G_1 = \frac{1}{120\pi^2}\int_0^{\pi}\left[\frac{\sin\left(\frac{k_0 W_p}{2}\cos\theta\right)}{\cos\theta}\right]^2 (\sin\theta)^3 d\theta \tag{13}$$

$$G_{12} = \frac{1}{120\pi^2}\int_0^{\pi}\left[\frac{\sin\left(\frac{k_0 W_p}{2}\cos\theta\right)}{\cos\theta}\right]^2 J_0(k_0 L_p \sin\theta)(\sin\theta)^3 d\theta \tag{14}$$

$$S_{11} = \frac{\frac{T_{11}+T_{12}}{Z_0 - T_{21}Z_0 - T_{22}}}{\frac{T_{11}+T_{12}}{Z_0 + T_{21}Z_0 + T_{22}}} \tag{15}$$

$$T = T_1 \cdot T_2 = \begin{bmatrix} \cosh\gamma l_1 & Z_1 \sinh\gamma l_1 \\ \frac{\sinh\gamma l_1}{Z_1} & \cosh\gamma l_1 \end{bmatrix}\begin{bmatrix} \cosh\gamma l_2 & Z_2 \sinh\gamma l_2 \\ \frac{\sinh\gamma l_2}{Z_2} & \cosh\gamma l_2 \end{bmatrix} \tag{16}$$

$$e = \frac{\sum_{f_n} \text{abs}(S_{11,f_n} - S_{11T})}{N} \tag{17}$$

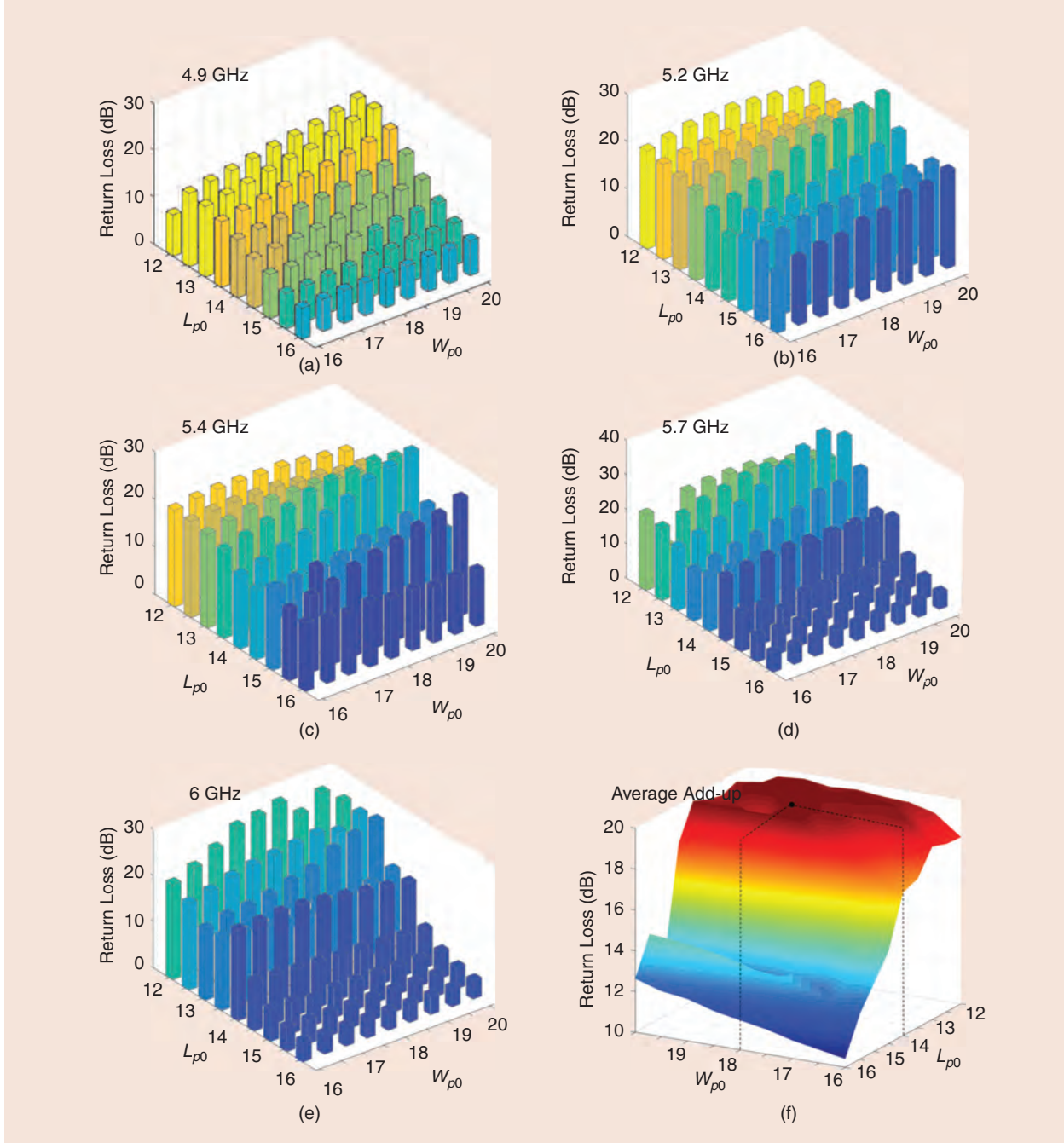

FIGURE 6. The return loss of the demonstrative stretchable patch antenna evaluated with all reasonable combinations of the initial patch length of L_p and width of W_p: (a) 4.9 GHz, (b) 5.2 GHz, (c) 5.4 GHz, (d) 5.7 GHz, (e) 6.0 GHz. (f) Evaluated average added-up results at all frequencies.

where k_0 is the wavenumber and J_0 is the zero-order Bessel function of the first kind. The calculated value of the input impedances $Zp(f)$ array is $\{Z_p(f_1) = 400.01\ \Omega, Z_p(f_2) = 354.3\ \Omega, Z_p(f_3) = 322.6\ \Omega, Z_p(f_4) = 281.6\ \Omega, Zp(f_5) = 257.4\ \Omega\}$. For the two-order microstrip impedance matching line with a reactance groove chosen as the feedline of the stretchable patch antenna shown in Figure 2(b), six-dimension parameters can be determined by using impedance matching optimization. The return loss S_{11} at the input port can be derived based on the transmission matrices T of the feedline shown in (15), and the expression of T shown in (16), where T_1, T_2, Z_1, and Z_2 are the transmission matrix and the characteristic impedances of the first and the second order of the feedline, respectively. Then, the weighted error function e shown in (17) is defined as the convergence condition with a targeted return loss S_{11T} of 20 dB, where parameter N is the number of discrete sampled frequency points f_n.

The optimized initial dimensions of the feedline structure are as follows: $MW_{10} = 1.7$ mm, $MW_{20} = 0.8$ mm, $ML_{10} = 2.6$ mm, $ML_{20} = 7$ mm, $PW_{10} = 14.5$ mm, and $PL_{10} = 0.6$ mm, respectively. After the initial dimensions and the strain ratio calculating, a complete strain involved 3D model in HFSS is still necessary to validate the design.

ANTENNA SIMULATION AND PERFORMANCE VALIDATION

In conventional designs of a soft antenna, only lengthwise change brought by strain ratio is considered [19], [20], [21]; relative dielectric constant and structure dimensions (W, H) are taken to be unchanged. To validate the proposed strain involved design method, the antenna is also designed by using a conventional method and simulated in HFSS. The simulated S-parameters S_{11} and the realized gain of the patch antenna under applied strain from 0 to 20% with and without using the proposed design are compared in Figure 7(a) and (b), respectively. In the legend, "ori" means 0% strain, "St5" means 5% strain, "St10" means 10% strain, "St15" means 15% strain, and "St20" means 20% strain, respectively. Prefix C means design using the conventional method.

In the conventional design route, the central frequency point 5.4 GHz (10% strain) is chosen as the main optimized frequency. The simulated result shows that the proposed antenna

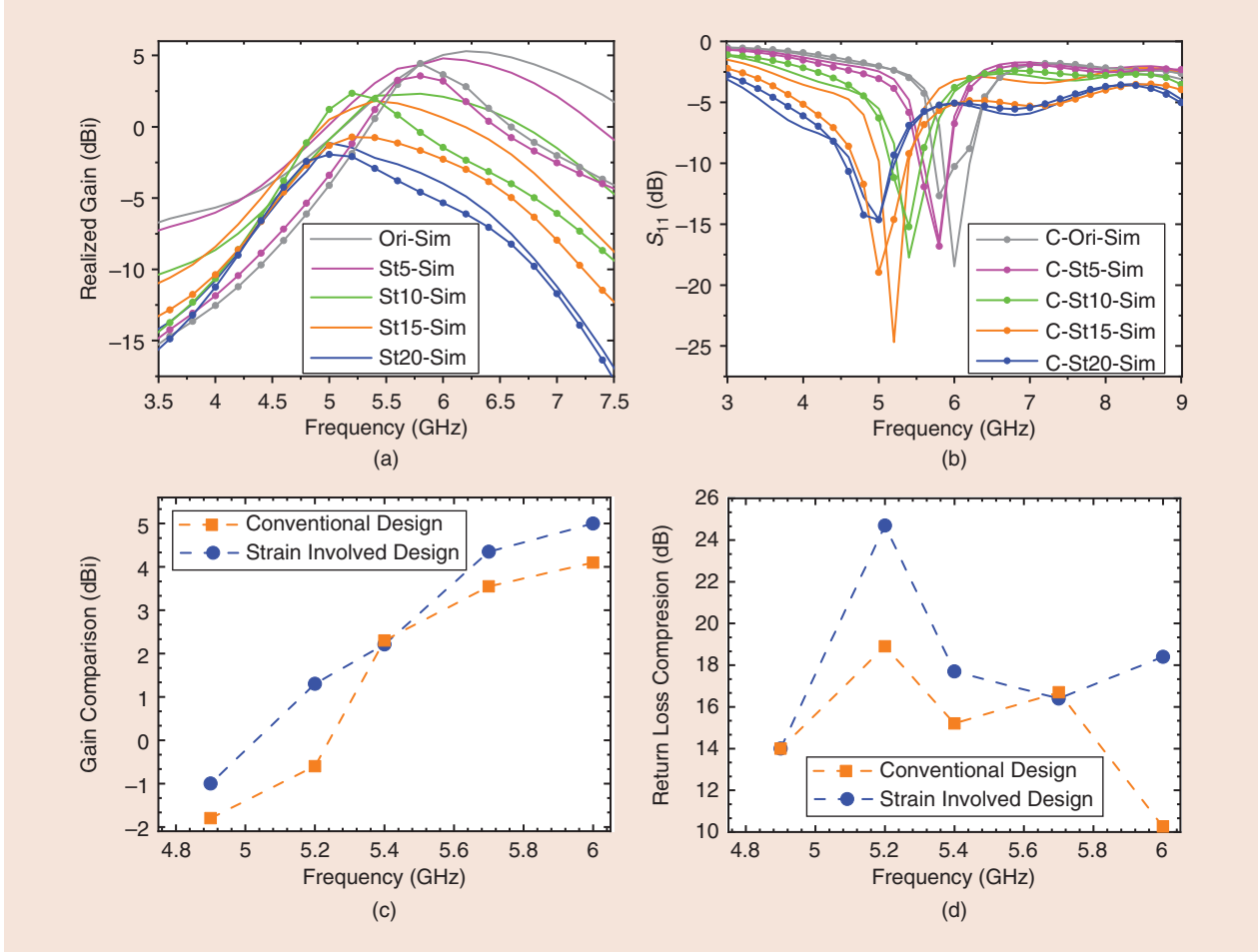

FIGURE 7. Comparison of the stretchable patch antenna performance designed by using the proposed method and conventional method. (a) The realized gain of the two patch antennas (in the legend, capital letter "C" means design using the conventional method). (b) The return loss of the two patch antennas. (c) The comparison of the realized gain at the five designed frequency points. (d) The comparison of the return loss at the five designed frequency points.

reliably achieves 2.2 dBi realized gain, which is 0.1 dBi lower than that of the antenna using the conventional design method. However, in other reconfigurable frequency points caused by stretching, except for the shifted operating frequency point, the maximal realized gains are decreased by 0.9 dBi (0% strain at 6 GHz), 0.9 dBi (5% strain at 5.7 GHz), 1.9 dBi (15% strain at 5.2 GHz), and 0.8 dBi (20% strain at 4.9 GHz), respectively, when using the conventional method.

EXPERIMENTAL RESULTS AND ANALYSIS

To evaluate the strain domain involved design method, the stretchable antenna was fabricated using the prestrain process and then the metal area was brushed with conductive silver paste. The photo of the stretchable antenna sample with 20% strain is displayed in Figure 8(a).

The electrical performance of the stretchable patch antenna was tested in a microwave anechoic chamber with a near-field testing system as shown in Figure 8(b). An RF signal was generated at one port of the vector network analyzer (ZNA43 from Rohde & Schwarz) and amplified by a power amplifier, then radiated outside of the stretchable antenna. The RF signal was then received by a standard probe. The fixture was away from the patch and kept out of the primary radiating direction, so its impact could be ignored.

The measured return losses, gains, and radiation patterns of the stretchable microstrip patch antenna under the relaxed and stretched states are shown in Figure 9. As shown in Figure 9(a), the measured patterns have a good agreement with the simulation data in the main beam lobe. As shown in Figure 9 (b) and (c), under different strain magnitudes, the operating frequency can be reconfigured. By stretching the antenna longitudinally, the central operating frequency can be tuned to 6, 5.4, or 5 GHz with the maximum realized gain gradually decreasing from 5.0 dBi to –0.1 dBi. The reason for this reduction is that the equivalent conductivity decreases with the stretching. Compared to the simulated data, there are about ±0.2 dB error in the reconfigured (poststrained) points. The primary reason for this discrepancy is due to the cracking in the Au/Ni metal bilayer caused by the applied strain. Compared to the simulated center frequency points, which are at 6, 5.4, and 4.9 GHz, the measured center frequency points drift slightly to 5.95 GHz (relaxed status), 5.45 GHz (with a strain of 10%), and 4.95 GHz (with a strain of 20%), respectively. As shown in Figure 9(d), the measured total efficiency is higher than the simulated result under 20% strain state. The reason is that we brushed the metal surface with the silver paste, which repaired the cracks and improved the conductivity of the stretchable metal layer.

Compared to the conventional patch antenna design, the optimal initial physical dimensions can be calculated with considerations of performance with respect to both frequency and strain change.

A comparison of the main performance of the designed stretchable antenna with several reported state-of-the-art works are summarized in Table 1.

CONCLUSIONS AND DISCUSSION

A general design route involving the strain domain for a reconfigurable microstrip patch antenna on a PDMS soft substrate is proposed and demonstrated. Conductivity of the conductor layer and the relative dielectric constant of the PDMS substrate under varied magnitudes of strain are investigated. Moreover, the deformation parameters of the soft antenna are simulated and analyzed. Then, variations of electrical and structural parameters are integrated into the equations and simulation model. Compared to the conventional patch antenna design, the optimal initial physical dimensions can be calculated with considerations of performance with respect to both frequency and strain change. Following the proposed design route, the measurement results of an example antenna show desired and controlled frequency reconfigurability with strain variation. The electrical performance perfectly matches the simulation data, which validates the reliability of the design route. The strain domain

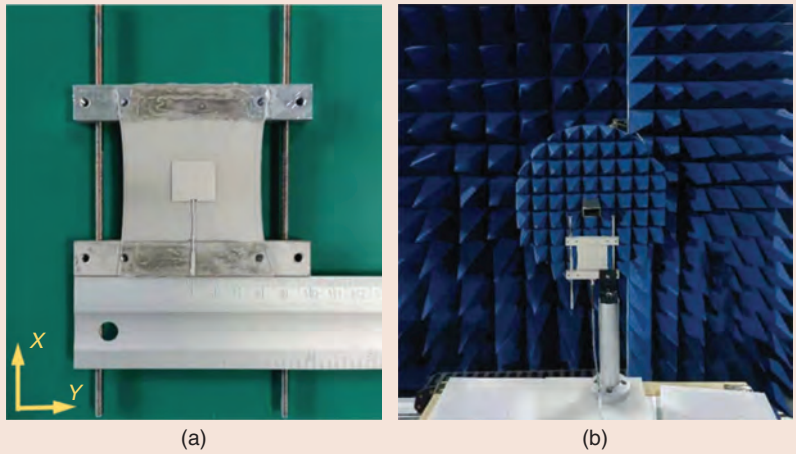

FIGURE 8. Stretch testing and radiation properties measurement scenario for the two antennas. (a) The stretchable microstrip patch antenna. (b) Near-field testing system.

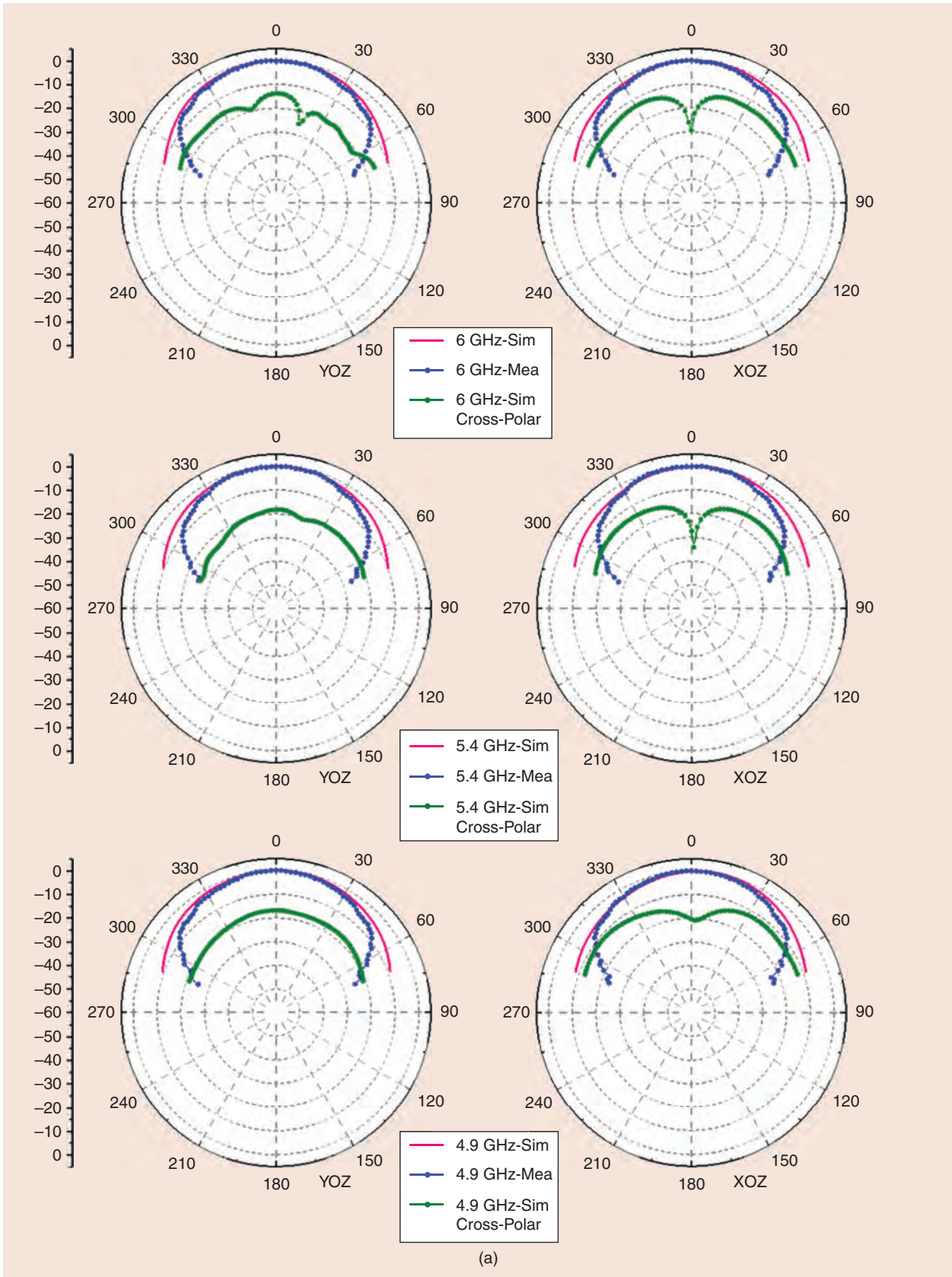

FIGURE 9. Experimental data compared with simulation results for the stretchable microstrip patch antenna. (a) Radiation patterns and cross-polarization levels on the *XOZ*-plane and the *YOZ*-plane in relaxed states (6 GHz), stretched state with an applied strain of 10% (5.4 GHz), and strain of 20% (4.9 GHz), respectively. (*Continued*)

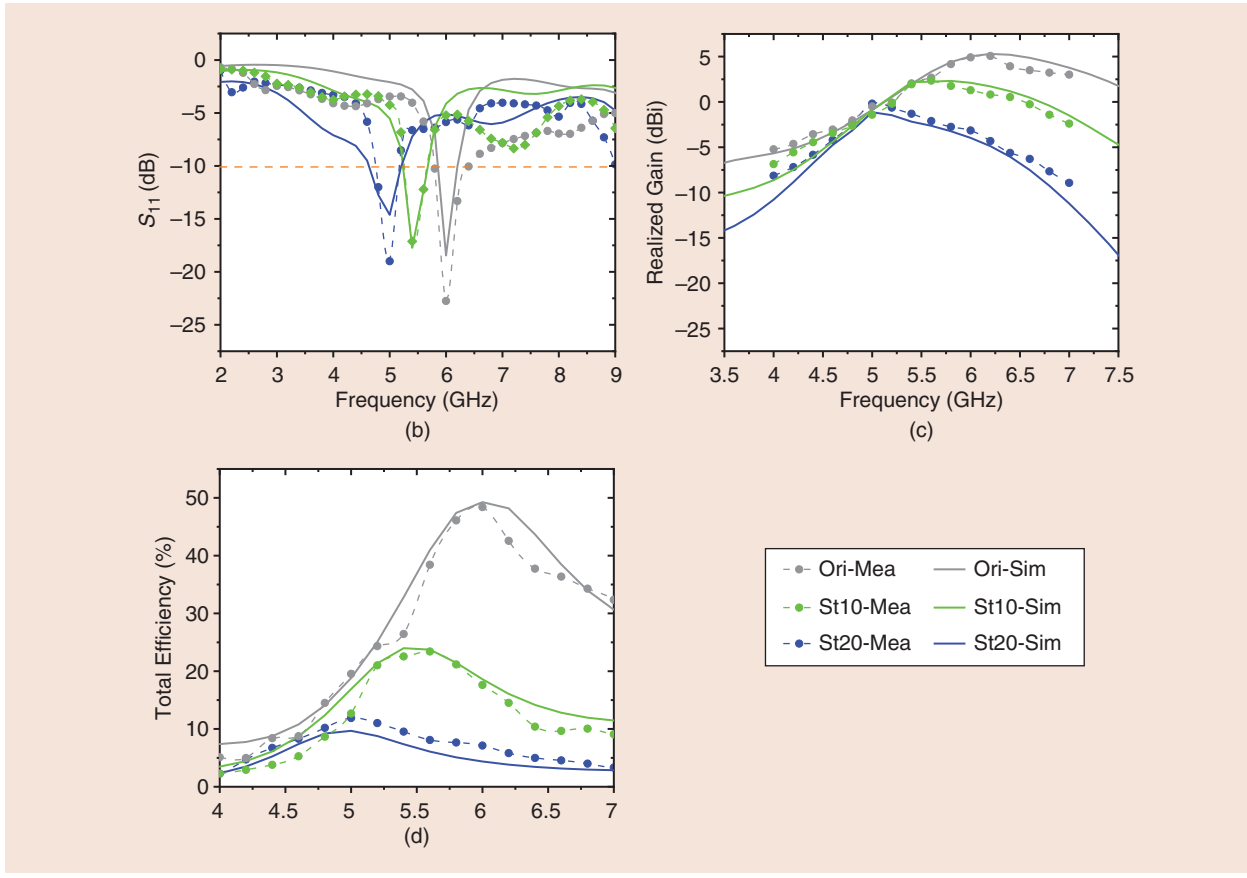

FIGURE 9. (*Continued*) Experimental data compared with simulation results for the stretchable microstrip patch antenna. (b) Reflection coefficients. (c) Realized gain. (d) Total efficiency.

involved design route for soft antennas can also be a good paradigm to the design of other soft microwave devices. The reduction of gain and efficiency caused by the conductivity decline could be improved using more ductile conductive materials like nanotube, graphene, and AgI-based composites.

As a method to realize reconfigurable performance, the stretchable antenna may have some irreplaceable advantages and practical usage, such as the following:

- The reconfigurable method is simple and compatible with additional control circuits.

TABLE 1. COMPARISON WITH RELEVANT LITERATURE.

Reference	Size	Frequency (GHz)	Relative Bandwidth (%)	Maximum Gain (dBi)	Maximum Efficiency (%)	Preset Frequency Before
[2]	0.39λ*0.0 2λ*0.004λ	1.56–1.7	8.6	2.14	90	No
[11]	0.155λ*0.155λ*0.073λ	0.17–0.47	95.33	5	94.4	No
[17]	0.32λ*0.32λ*2.584λ	4.3–5.3	21.2	14.4	N/A	No
[18]	2.15λ*2.15λ*0.036λ	1.3–3	79.07	6.1	80	No
[19]	0.427λ*0.27λ*0.021λ	0.78–2.42	102.5	2.8	72	No
[20]	0.974λ*0.42λ*0.012λ	6.2–6.4	3.17	2.17	N/A	No
[24]	0.113λ*0.081λ*0.004λ	2.46–2.94	17.78	–0.02	81.4	No
[25]	0.859λ*0.516λ*0.241λ	4.66–5.65	19.2	4.1	64	No
This work	0.13λ*0.12λ*0.002λ	4.9–6	20.18	5.0	48	Yes

λ: Free space wavelength at center frequency point.

- The stretchable antennas are more suitable to wearable devices compared to bendable antennas.
- The working frequency point is directly related to the deformation. So, the stretchable antenna is able to be used in posture recognizing, deformation monitoring, gesture controlling, and other wireless application scenarios.

ACKNOWLEDGMENT

This work was supported by the National Key Research and Development Program of China (2021YFA0715301). Wen Huang is the corresponding author.

AUTHOR INFORMATION

Lei Sang (sanglei2008@126.com) is with the School of Microelectronics, Hefei University of Technology, Hefei 230009, China. He is a Senior Member of IEEE.

Shuaitao Li (1275523508@qq.com) is with the School of Microelectronics, Hefei University of Technology, Hefei 230009, China.

Bin Hu (2020111239@mail.hfut.edu.cn) is with the School of Microelectronics, Hefei University of Technology, Hefei 230009, China.

Kehan Dai (2557732213@qq.com) is with the School of Microelectronics, Hefei University of Technology, Hefei 230009, China.

Mark Kraman (mkraman2@illinois.edu) is with the Department of Electrical and Computer Engineering, University of Illinois at Urbana-Champaign, Champaign, IL 61801, USA.

Hong Yang (yanghong@cesi.cn) is with the China Electronics Standardization Institute, Beijing 100007, China.

Wen Huang (huangw@hfut.edu.cn) is with the School of Microelectronics, Hefei University of Technology, Hefei 230009, China. He is a Senior Member of IEEE.

REFERENCES

[1] L. H. Blumenschein et al., "A tip-extending soft robot enables reconfigurable and deployable antennas," *IEEE Robot. Autom. Lett.*, vol. 3, no. 2, pp. 949–956, Apr. 2018, doi: 10.1109/LRA.2018.2793303.

[2] J. C. Prather et al., "Biomimetic antenna design for an airborne atmospheric probe," *IEEE Trans. Antennas Propag.*, vol. 67, no. 1, pp. 48–55, Jan. 2019, doi: 10.1109/TAP.2018.2874773.

[3] A. Kiourti, "RFID antennas for body-area applications: From wearables to implants," *IEEE Antennas Propag. Mag.*, vol. 60, no. 5, pp. 14–25, Oct. 2018, doi: 10.1109/MAP.2018.2859167.

[4] K. Guido et al., "Tissue-emulating phantoms for in vitro experimentation at radio frequencies: Exploring characteristics, fabrication, and testing methods," *IEEE Antennas Propag. Mag.*, vol. 63, no. 6, pp. 29–39, Dec. 2021, doi: 10.1109/MAP.2020.3003208.

[5] M. Ramuz et al., "Transparent, optical, pressure-sensitive artificial skin for large-area stretchable electronics," *Adv. Mater.*, vol. 24, no. 24, pp. 3223–3227, Jun. 2012, doi: 10.1002/adma.201200523.

[6] B. C.-K. Tee et al., "A skin-inspired organic digital mechanoreceptor," *Science*, vol. 350, no. 6258, pp. 313–316, Oct. 2015, doi: 10.1126/science.aaa9306.

[7] A. J. Palma et al., "Comparison of fabrication techniques for flexible UHF RFID tag antennas," *IEEE Antennas Propag. Mag.*, vol. 59, no. 5, pp. 159–168, Jun. 2017, doi: 10.1109/MAP.2017.2731214.

[8] F. Mokhtari-Koushyar et al., "A miniaturized tree-shaped fractal antenna printed on a flexible substrate: A lightweight and low-profile candidate with a small footprint for spaceborne and wearable applications," *IEEE Antennas Propag. Mag.*, vol. 61, no. 3, pp. 60–66, Jun. 2019, doi: 10.1109/MAP.2019.2907878.

[9] A. E. Serebryannikov et al., "Ultraminiature antennas combining subwavelength resonators and a very-high-ε uniform substrate: The case of lithium niobate," *IEEE Trans. Antennas Propag.*, vol. 68, no. 7, pp. 5071–5081, Jul. 2020, doi: 10.1109/TAP.2020.2975544.

[10] Y. Sen et al., "Wearable dual-band magneto-electric dipole antenna for WBAN/WLAN applications," *IEEE Trans. Antennas Propag.*, vol. 63, no. 9, pp. 4165–4169, Sep. 2015, doi: 10.1109/TAP.2015.2443863.

[11] L. Xing et al., "A high-efficiency wideband frequency-reconfigurable water antenna with a liquid control system: Usage for VHF and UHF applications," *IEEE Antennas Propag. Mag.*, vol. 63, no. 1, pp. 61–70, Feb. 2021, doi: 10.1109/MAP.2019.2946556.

[12] Y. Shafiq et al., "A reusable battery-free RFID temperature sensor," *IEEE Trans. Antennas Propag.*, vol. 67, no. 10, pp. 6612–6626, Oct. 2019, doi: 10.1109/TAP.2019.2921150.

[13] G. S. Guvanasen et al., "A stretchable microneedle electrode array for stimulating and measuring intramuscular electromyographic activity," *IEEE Trans. Neural Syst. Rehabil. Eng.*, vol. 25, no. 9, pp. 1440–1452, Sep. 2017, doi: 10.1109/TNSRE.2016.2629461.

[14] E. Siman-Tov et al., "Increasing the range of wireless power transmission to stretchable electronics," *IEEE Trans. Microw. Theory Techn.*, vol. 66, no. 11, pp. 5021–5030, Nov. 2018, doi: 10.1109/TMTT.2018.2859948.

[15] S. D. Wang et al., "Mechanical designs for inorganic stretchable circuits in soft electronics," *IEEE Trans. Compon. Packag. Manuf. Technol.*, vol. 5, no. 9, pp. 1201–1208, Sep. 2015, doi: 10.1109/TCPMT.2015.2417801.

[16] S. K. Behera and N. C. Karmakar, "Wearable chipless radio-frequency identification tags for biomedical applications: A review," *IEEE Antennas Propag. Mag.*, vol. 62, no. 3, pp. 94–104, Jul. 2020, doi: 10.1109/MAP.2020.2983978.

[17] C. Xu, Z. Wang, Y. Wang, P. Wang, and S. Gao, "A polarization-reconfigurable wideband high-gain antenna using liquid metal tuning," *IEEE Trans. Antennas Propag.*, vol. 68, no. 8, pp. 5835–5841, Aug. 2020, doi: 10.1109/TAP.2020.2996773.

[18] A. Kiourti and J. L. Volakis, "Stretchable and flexible E-fiber wire antennas embedded in polymer," *IEEE Antennas Wireless Propag. Lett.*, vol. 13, no. 7, pp. 1381–1384, Jul. 2014, doi: 10.1109/LAWP.2014.2339636.

[19] F. Xie, J. J. Adams, and M. S. Tong, "An UHF reconfigurable liquid-metal monopole antenna based on a 2-D surface," *IEEE Trans. Compon. Packag. Manuf. Technol.*, vol. 11, no. 11, pp. 1980–1987, Nov. 2021, doi: 10.1109/TCPMT.2021.3116056.

[20] S. J. Mazlouman et al., "A reconfigurable patch antenna using liquid metal embedded in a silicone substrate," *IEEE Trans. Antennas Propag.*, vol. 59, no. 12, pp. 4406–4412, Dec. 2011, doi: 10.1109/TAP.2011.2165501.

[21] C. P. Lin et al., "Development of a flexible SU-8/PDMS-based antenna," *IEEE Antennas Wireless Propag. Lett.*, vol. 10, pp. 1108–1111, Oct. 2011, doi: 10.1109/LAWP.2011.2170398.

[22] K. Pan et al., "Soft wireless battery-free UHF RFID stretchable sensor based on microfluidic technology," *IEEE J. Radio Freq. Identif.*, vol. 3, no. 4, pp. 252–258, Dec. 2019, doi: 10.1109/JRFID.2019.2912959.

[23] C. Wang et al., "Design of a reconfigurable patch antenna using the movement of liquid metal," *IEEE Antennas Wireless Propag. Lett.*, vol. 17, no. 6, pp. 974–978, Jun. 2018, doi: 10.1109/LAWP.2018.2827404.

[24] T. Jang et al., "Semitransparent and flexible mechanically reconfigurable electrically small antennas based on tortuous metallic micromesh," *IEEE Antennas Wireless Propag. Lett.*, vol. 65, no. 1, pp. 150–158, Jan. 2017, doi: 10.1109/TAP.2016.2623479.

[25] Z. P. Zhong et al., "A 3D-printed hybrid water antenna with tunable frequency and beamwidth," *Electronics*, vol. 7, no. 10, Oct. 2018, Art. no. 230, doi: 10.3390/electronics7100230.

[26] S. Cheng and Z. Wu, "A microfluidic, reversibly stretchable, large-area wireless strain sensor," *Adv. Functional Mater.*, vol. 21, no. 12, pp. 2282–2290, Jun. 2011, doi: 10.1002/adfm.201002508.

[27] Z. Li et al., "Rational design of a printable, highly conductive silicone-based electrically conductive adhesive for stretchable radio-frequency antennas," *Adv. Functional Mater.*, vol. 25, no. 3, pp. 464–470, Jan. 2015, doi: 10.1002/adfm.201403275.

[28] S. Zhao, Y. Zhang, and J. Yang, "Improving interfacial shear strength between graphene sheets by strain-induced wrinkles," *Carbon*, vol. 168, pp. 135–143, Oct. 2020, doi: 10.1016/j.carbon.2020.06.054.

[29] Z. L. Li et al., "Interfacial stress transfer in strain engineered wrinkled and folded graphene," *2D Mater.*, vol. 6, no. 4, pp. 2053–2059, Jul. 2019, doi: 10.1088/2053-1583/ab3167.

[30] O. Akogwu et al., "Large strain deformation and cracking of nano-scale gold films on PDMS substrate," *Mater. Sci. Eng., B*, vol. 170, nos. 1–3, pp. 32–40, Jun. 2010, doi: 10.1016/j.mseb.2010.02.023.